International Journal of Technology 11(1) 81-90 (2020)
Received April 2019 / Revised November 2019 / Accepted January 2020

International Journal of Technology

http://ijtech.eng.ui.ac.id

Spray Angle Dependence for the Growth of Terrace-truncated Nanocone Structure of Gallium-doped Zinc Oxide by Advanced Spray Pyrolysis Deposition Technique

Sameera Attanayake[1*], Masayuki Okuya[2], Kenji Murakami[2]

[1]*Graduate School of Science and Technology, Shizuoka University, Hamamatsu 432-8011, Japan*
[2]*Graduate School of Integrated Science and Technology, Shizuoka University, Hamamatsu 432-8011, Japan*

Abstract. Rough-surfaced nanocone structures are preferred for use as transparent conductive oxides due to their high optical transparency and electrical conductivity. Structural properties of Ga-doped ZnO terrace-truncated nanocones, which were grown by advanced spray pyrolysis deposition technique, vastly changes with the spraying angle. In the present study, the effect of the spray angle on terrace-truncated nanocone structure formation was investigated. Spray pyrolysis deposition technique was used to grow the nanostructure as the growth rate can be controlled easily. The prepared samples were characterized using X-ray diffraction spectroscopy (XRD) and scanning electron microscopy (SEM) techniques. Optical and electrical properties were investigated by the UV-visible spectrum and four-probe method. The lowest spray angle of 15º showed homogeneous and hexagonal shaped nanocone structure with an average top diameter of 22.8 nm and an average height of 240 nm. An excellent transparent conductive oxide behavior was obtained from the sample synthesized at the lowest spray angle of 15º with high conductivity of $2.5\times10^3\ \Omega^{-1}.cm^{-1}$ and high transparency of 82% in the visible range.

Keywords: Ga-doped ZnO; Spray angle; Spray pyrolysis; Terrace-truncated nanocone structure; Transparent conductive oxide material

1. Introduction

Semiconductor oxides, which have high electrical conductivity as well as high transparency in the visible range, are considered transparent conductive oxide (TCO) materials. They have a wide range of commercial applications such as smart devices, liquid crystal displays (LCDs), light emitting diodes (LEDs), touch panels, etc. (Wu et al., 2008; Liu et al., 2010; Yan et al., 2015). In general, ITO, SnO_2, Ga_2O_3, In_2O_3, and CdO are extensively used as TCO materials. Among them, ITO is the most well-established TCO material as it has excellent transparent conducting performances.

However, there is a high demand for new TCO materials due to the scarcity and lower stability of indium in hydrogen plasma. Impurity-doped ZnO is commonly used as an optional TCO material, as an alternative to ITO (Look, 2001; Rao and Kumar, 2010; Bedia et al., 2014; Bramantyo et al., 2019). ZnO is an n-type II-VI semiconductor with unique physical and chemical properties such as direct wide band gap (3.37 eV), large exciting binding energy at room temperature (~60 meV), high thermal stability, and nontoxicity (Yim et al.,

*Corresponding author's email: a.m.s.l.b.attanayake@shizuoka.ac.jp
doi: 10.14716/ijtech.v11i1.3068

2007; Fernández and Gandía, 2012; Moditswe et al., 2016). The conductivity of ZnO is caused by ionization of zinc interstitials and oxygen vacancies. The carrier formation by ionization of Zn interstitial is the preponderant mechanism for intrinsic ZnO (Yim et al., 2007). To enhance the electrical conductivity and optical transparency, ZnO is doped with impurities such as B, Al, Ga, Sn, Y, Sc, Ti, or Zr (Look, 2001; Yim et al., 2007; Rao and Kumar, 2010; Moditswe et al., 2016). Even though Al and Ga attained the dominant attention as dopants for ZnO, Ga is considered the preferable dopant because of its similarity in both covalent and ionic radii (0.62 Å and 1.26 Å) with that of Zn (0.74 Å and 1.31 Å) (Bedia et al., 2014). Moreover, covalent bond length of Ga–O (1.92 Å) is comparable with the covalent bond length of Zn–O (1.97 Å) with respect to Al–O (2.7 Å) and In-O (2.1 Å) (Le et al., 2010). Because of this, lattice distortion is possessed at a minimal value even ZnO is highly doped with Ga (Look, 2001). Moreover, when comparing with Al, Ga has high electronegativity, high stability to moisture, and lower reactivity and diffusivity (Look, 2001; Fernández and Gandía, 2012). It is considered that doped Ga atoms replace Zn host atoms and expand free electron density, which increases the electrical conductivity. There are many reports on the formation of various kinds of impurity-doped ZnO structures, such as nanorods, nanoflakes, nanobelts, nanoparticles, nanocones, etc. Among them, it is widely accepted that the 1-D nanorod structure is the most suitable layout for dye sensitized solar cell applications because of its high surface-to-volume ratio.

However, some researchers have reported about the importance of ZnO nanocone structure, which could increase the light transparency with respect to nanorods, by reducing the scattering (Lao et al., 2003; Gao et al., 2006; Yin et al., 2012; Li et al., 2015; Han et al., 2018). Various methods have been developed to produce ZnO thin films, such as pulsed laser deposition, metal-organic chemical vapor deposition (MOCVD), spray pyrolysis, sputtering, sol-gel, and chemical bath deposition techniques (Hu and Gordon, 1992; Hirata et al., 1996; Chen et al., 1998; Sholehah and Yuwono, 2015). Spray pyrolysis deposition (SPD) technique has several advantages over other methods, such as simplicity, low cost, ability for large area deposition, and high homogeneity (Yadav et al., 2010). One of the most important advantages of SPD technique is its ability to change the growth rate easily.

In this study, we have used the rotational, pulsed, and atomized spray pyrolysis deposition technique (RPASP). This method has numerous advantages over normal spray pyrolysis deposition techniques as we can optimize the device according to the requirements by changing the parameters. This novel device is capable of individually controlling spray time, time interval during each spray, rotation speed, number of rotations, distance between the nozzle tip and glass substrate, and spray angle. In general, the spray angle is considered as a critical factor in spray pyrolysis deposition technique. Bandara et al. (2016) also reported about the importance of spray angle for the growth of fluorine-doped zinc oxide 1-D nanostructures. In this study, we have investigated the effect of spray angle for the growth and properties of terrace-truncated nanocone structure of Ga-doped ZnO by RPASP deposition technique, as no proper study has been reported to the best of our knowledge.

2. Methods

Zinc acetate dihydrate (Wako Pure Chemical Industries, Ltd., Osaka, Japan) was dissolved in 100 mL of 2-methoxyethanol (Wako Pure chemicals) to obtain 0.5 mol dm^{-3} of Zn^{2+} solution. Ten drops of ethanolamine (Sigma Aldrich) was added as a stabilizer while stirring the mixture. Ga $(NO_3)_3.xH_2O$ (Wako Pure Chemicals, Ga/Zn ratio: 2 at %) was added for doping. The solution was stirred for 60 min at 70°C and aged for 24 hours at room

temperature. Commercially available fluorine-doped tin oxide (FTO) glasses (2.5 cm × 2.5 cm) were ultrasonically cleaned in a mixture of acetone, ethyl alcohol, and distilled water. Thickness of the FTO layer was 500 nm. Finally, the precursor solution was deposited by using advanced spray pyrolysis deposition technique. The deposition temperature was set to 400°C. The distance between the nozzle tip and FTO substrate was kept constant at 0.5 cm. The spray pressure was set to 0.40 MPa and spraying was continued for 2 s in 12 s time intervals. Total spray time was 160 min and the spraying angle was varied by changing the nozzle direction as shown in Table 1. The crystal structure was characterized by using X-ray diffractometer (Rigaku RINT Ultima-III at 40 kV with Cu K_α radiation λ = 1.541836 Å). The XRD spectra were acquired in the range of 30º–80º. The surface morphology was examined by field emission scanning electron microscope (JEOL JSM-6320F) with an acceleration voltage of 15 keV, accompanying energy dispersive X-ray spectroscopy. The layer thickness was measured by cross-sectional FE-SEM images.

Table 1 Spraying angles and volumes of Ga-doped ZnO samples

Sample	Spraying Angle	Spraying Volume (ml)
Ga-ZnO/15º–100 ml	15º	100
Ga-ZnO/30º–100 ml	30º	100
Ga-ZnO/45º–100 ml	45º	100
Ga-ZnO/15º–200 ml	15º	200

The UV-visible transmission spectra were obtained by JASCO V-630 spectrometer in the wavelength range of 300–800 nm. Electrical characteristics of prepared samples were obtained by four probe method of Hall effect measurement system, HMS-3000.

3. Results and Discussion

Figure 1 shows the FE-SEM image of Ga-ZnO/15º–100 ml sample. In this structure, the average top diameter, and the height were 22.8 nm and ~240 nm, respectively. The nanostructure density of this sample was 195 per μm^2.

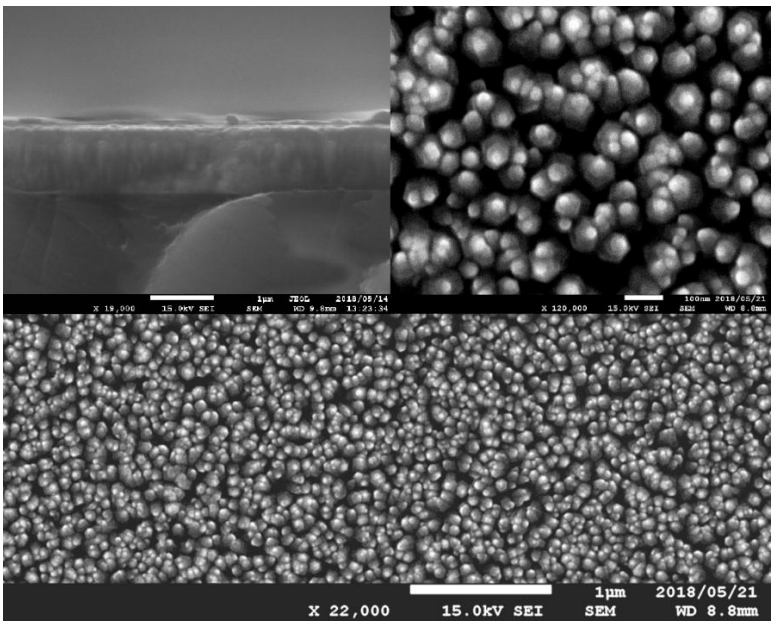

Figure 1 FE-SEM images of Ga-doped ZnO nanostructure at 15º spray angle

Figure 2a shows the FE-SEM image of Ga-ZnO/30°–100 ml sample, with a nanostructure of an average top diameter of 36.9 nm and average height of ~220 nm. The nanostructure density of the sample was 230 per μm². Figure 2b shows the FE-SEM image Ga-ZnO/45°–100 ml sample. The observed nanostructure has an average top diameter of 38.3 nm and the sample has 138 per μm² of nanostructure density. Nano plates were observed in between the nanostructures, which interferes with their further growth.

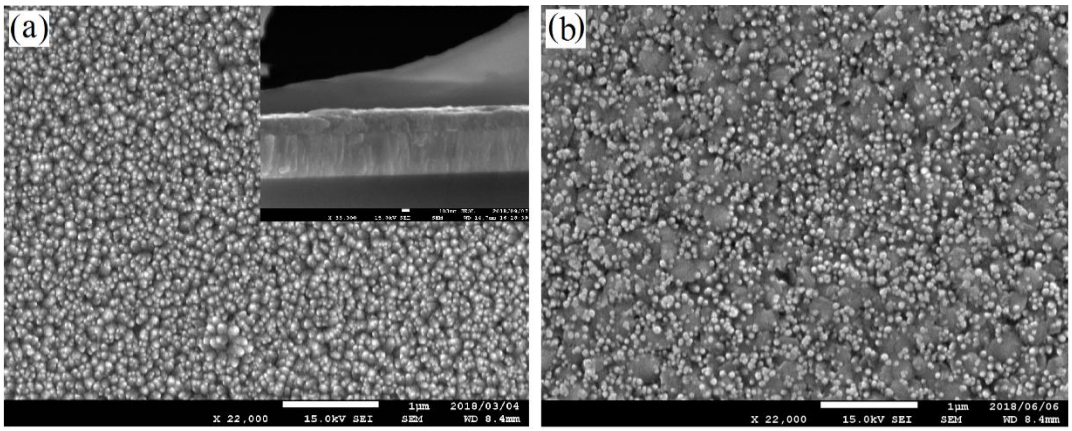

Figure 2 FE-SEM images of Ga-doped ZnO nanostructure at spray angles of: (a) 30° and (b) 45°

According to the FE-SEM images, Ga-ZnO/15°–100 ml sample shows a more favorable structure for a transparent conductive oxide material with respect to other samples because of low structural defects and high homogeneity. However, the shape of the nanostructure could not be confirmed at this stage. Figure 3 represents the velocity and forces acting on a certain vaporized particle that was sprayed through the nozzle. Here, we assume the drag force by air molecules is zero and there is no loss of energy after the collision with the FTO glass substrate (perfectly elastic collision), as our purpose is to compare the impact at each spraying angle. Moreover, it is assumed that the potential energy gained by a particle is similar at all spray angles, as the nozzle height was kept constant throughout the process.

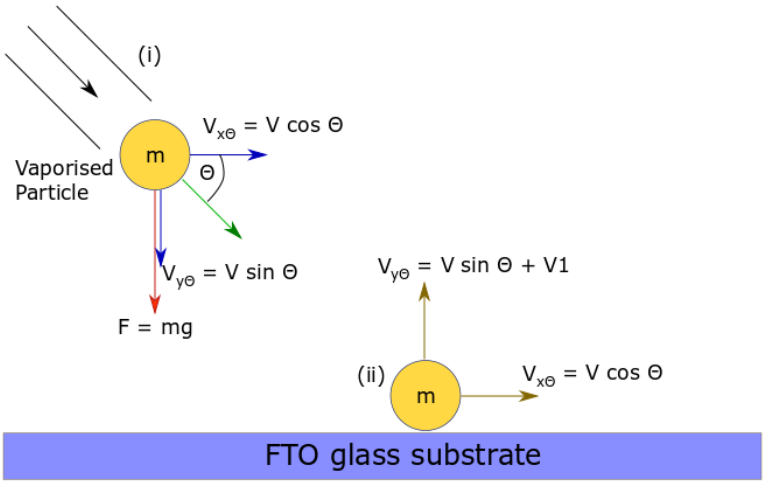

Figure 3 Simulation-velocity and forces acting on a vaporized particle, which was sprayed at Θ angle; (i) just after ejection from the nozzle, and (ii) just after collision with the substrate

$V_{x\theta}$ and $D_{x\theta}$ are horizontal components of velocity and displacement at spraying angle of θ, respectively. Vy_{θ} and $D_{y\theta}$ are vertical components of velocity and displacement at spraying angle of θ, respectively. $V1$ is the velocity gained by the particle due to potential energy, which does not change with the spraying angle, θ. When the particle is at the position (ii) as shown in Figure 3, following relationships can be derived:

$\theta = 15^{o}$,

$$V_{x15} = V \text{ Cos } 15^{o} \quad (1)$$

$$V_{y15} = V \text{ Sin } 15^{o} + V1 \quad (2)$$

$\theta = 30^{o}$,

$$V_{x30} = V \text{ Cos } 30^{o} \quad (3)$$

$$V_{y30} = V \text{ Sin } 30^{o} + V1 \quad (4)$$

$\theta = 45^{o}$,

$$V_{x45} = V \text{ Cos } 45^{o} \quad (5)$$

$$V_{y45} = V \text{ Sin } 45^{o} + V1 \quad (6)$$

By considering Equations 1–6, we can say that $V_{x15} > V_{x30} > V_{x45}$ and $V_{y45} > V_{y30} > V_{y15}$; and, therefore, as the displacement increases with velocity, $D_{x15} > D_{x30} > D_{x45}$ and $Dy_{45} > D_{y30} > D_{y15}$. Thus, from the above, we can state that the horizontal velocity and displacement are decreasing, while increasing the vertical velocity and displacement, with the spraying angle. Figure 5 illustrates the projectile movement of a random particle at each spraying angle.

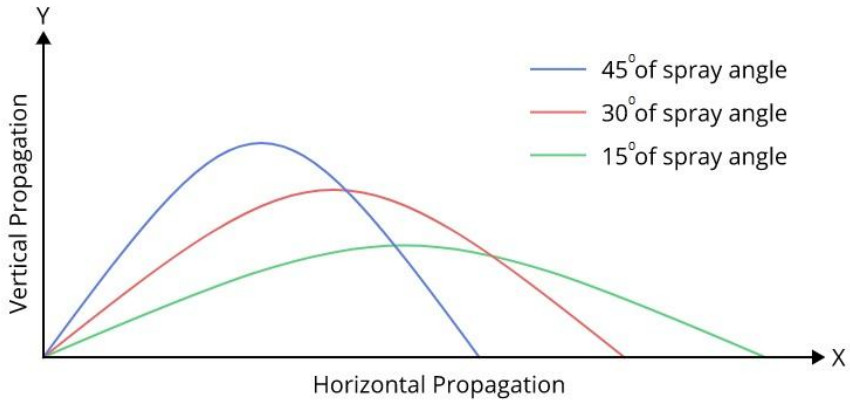

Figure 4 Projectile movement of a vaporized particle at each spraying angle

At lower spraying angles, particles travel longer distance horizontally and shorter vertically. Because of this phenomenon, particles disperse and spread all over the glass substrate and finally produce an excellent homogeneous layer. On the other hand, at higher spraying angles, particles travel longer distance vertically and shorter distance horizontally, thus narrowing the spraying area. At higher spraying angles, the vaporized particles deposit on top of each other forming plate-like structures that were clearly visible in the FE-SEM images Figure 2b. We increased the spraying volume to investigate the nanostructure, as it was not clear until this point of the research. Figure 5 shows the FE-SEM images of Ga-ZnO/15^{o}–200 ml sample, which consist of proposed terrace-truncated nanocone structure.

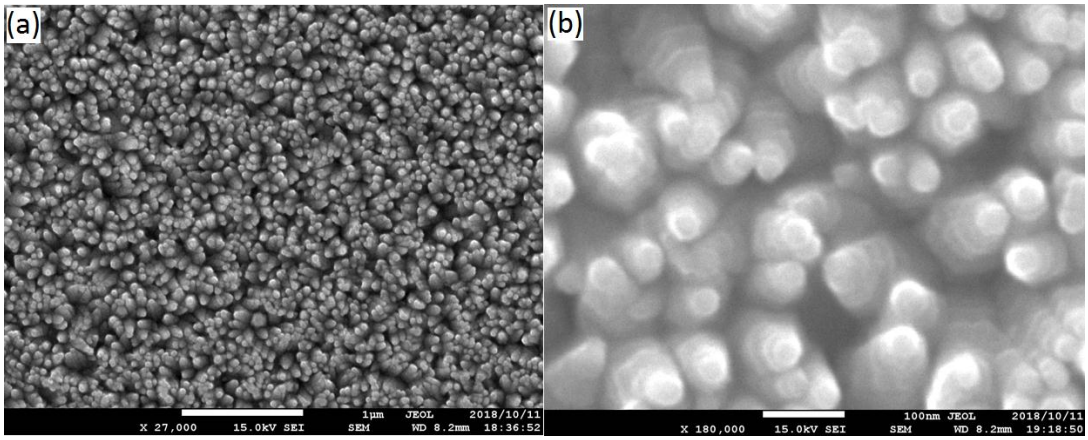

Figure 5 FE-SEM images of Ga-ZnO/15°–200 ml sample at magnifications of: (a) 27,000; (b) 180,000

Some researches have reported about the use of ZnO nanocone structures that increase the light transparency by reducing the scattering. In Ga-ZnO/15°–200 ml sample, the total spray time was 160 minutes consisting of 24 minutes of spraying time and 136 minutes of non-spray time. While spraying, we kept this long pause to regain the temperature, as the temperature of the glass substrate was reduced during the spraying. The high growth rate along the c-axis leads to a high decay rate in the same direction. The growth mechanism of nanocone structures is discussed in greatr detail by Rouhi et al. (2015) and suggests that it was due to the high growth rate along the (002) plane. We have described the growth mechanism of terrace-truncated nanocone structure in our previous paper (Attanayake et al., 2019). Rough-surfaced nanocone structures have lower top diameters that help in the transmision of light easily by reducing the scattering of light. On the other hand, nanorod structures have a higher light scattering rate, which reduce the transmittance. Optical transmittance might be higher in hexagonal nanocone structures, with respect to nanorods, according to the proposed light emission and scttering mechanism. These nanocone structures are suitable especially for light emitting diodes (LEDs) to increase their efficiency by decreasing the light extraction efficiency (LEE). Many reports have stated that, rough-bevel, cone-shaped hexagonal nano structure of ZnO has higher LEE, with respect to hexagonal nanorods of ZnO (Yin et al., 2012). Energy-dispersive X-ray (EDX) mapping images show the evidence for the uniform doping of Ga into ZnO crystal structure. According to literature, there is no effect of the dopant material (Ga) for the formation of terrace-truncated nanocones because similar structures were fabricated using pure ZnO (Rouhi et al., 2015; Visser et al., 2017).

Figure 6 shows the XRD patterns of Ga-doped ZnO that were grown using different spraying angles. Significant peak around 34.37° indicates the crystal structure was favored on (002) direction of hexagonal wurtzite ZnO phase (JCPDS card No. 36-1451), along the c-axis, perpendicular to the glass substrates, at all spray angles. The XRD spectra support the observations of FE-SEM images, as (002) peak intensity was decreased while increasing the spray angle. Ga-ZnO/15°–100 ml sample shows a weak peak around 72.5°, correspond to the (004) plane, which is a replica peak of (002). All the other peaks, which are marked with "•" originated from the FTO glass substrate. The crystallite sizes were calculated by using Scherrer equation which is shown in Equation 7.

$$D = \frac{0.9\lambda}{\beta cos\theta} \tag{7}$$

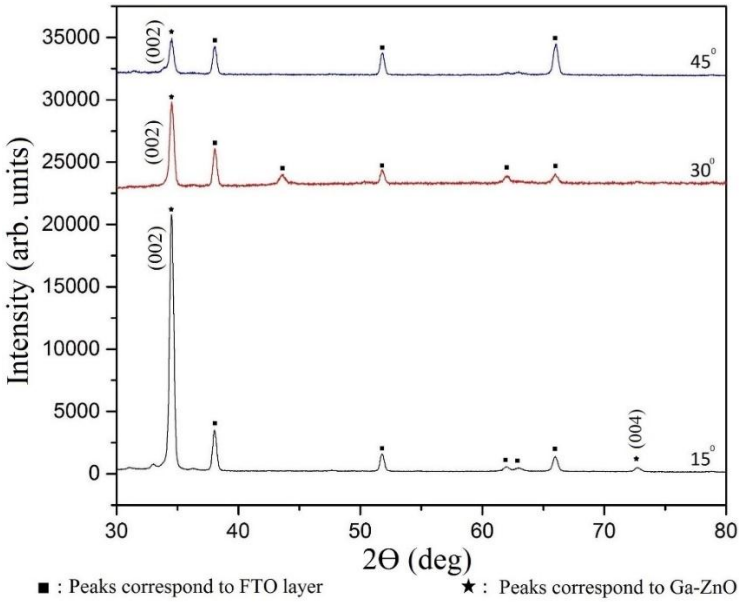

Figure 6 XRD patterns of Ga-doped ZnO thin films for each of the spray angles

where λ is the X-ray wavelength, β is the line broadening at half the maximum, and θ is the Bragg angle. The calculated crystallite sizes were 21.61, 21.84 and 21.80 nm for each of the spray angles 15°, 30°, and 45°, respectively. Figure 7 shows the UV-visible spectra of Ga-doped ZnO samples. The obtained optical transmittance in the visible range were 82%, 81%, and 79% in Ga-ZnO/15°–100 ml, Ga-ZnO/30°–100 ml, and Ga-ZnO/45°–100 ml samples, respectively. Optical transparency of the Ga-ZnO/45°–100 ml sample was lower than the typical transparency of a transparent conductive oxide material which is higher than 80%, due to the formation of plate-like structures.

Hsiao et al. (2013) also discussed the reduction of optical transmittance in the presence of wall-like structures. However, at lower spraying angle, high optical transmittance was observed due to the presence of terrace-truncated nanocone structure, as it minimizes the light scattering.

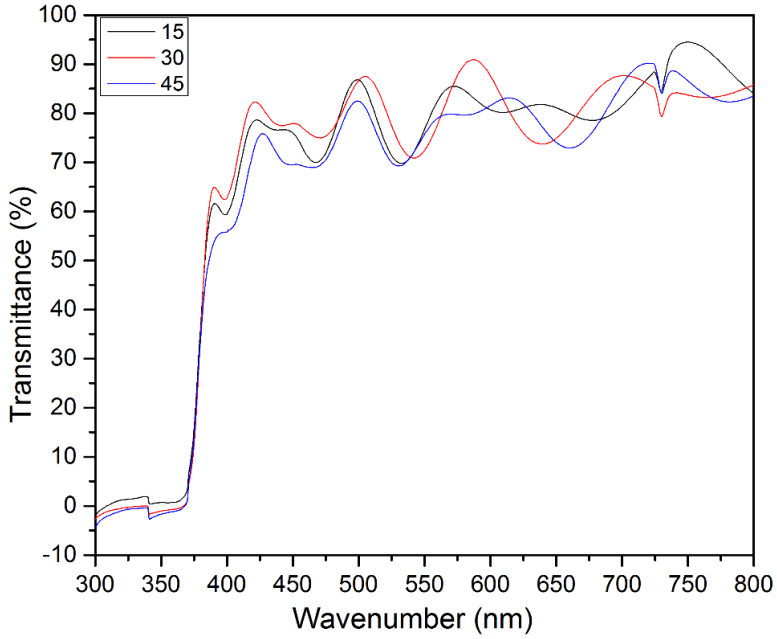

Figure 7 UV-visible spectra of Ga-doped ZnO thin films for each spray angle

Previous researches have shown that the optical transmittance of Ga-doped nanostructures is high in the visible range. The Ga-doped ZnO thin film with 85% of optical transmittance in the visible range was reported by Moditswe et al. (2016). In our structure, optical transmittance was not high as we expected, due to the two-layered FTO and Ga-doped ZnO structure, which leads to light scattering at layer boundaries. A transmittance peak around 300–340 nm was observed in all the samples, before the absorption edge. Ga-doped ZnO has n-type conductivity due to the oxygen vacancies, and zinc interstitials. The mobility, electrical conductivity, resistivity, and the bulk concentration of the prepared Ga-doped ZnO nanostructures are tabulated in Table 2.

Table 2 Mobility, conductivity, resistivity, and the bulk concentration of prepared Ga-doped ZnO samples

Sample	Mobility ($cm^2.V^{-1}.S^{-1}$)	Conductivity ($\Omega^{-1}.cm^{-1}$)	Resistivity (Ω. cm)	Bulk concentration (cm^{-3})
Bare FTO	18.13	3.7×10^{4}	2.7×10^{-4}	2.8×10^{20}
Ga-ZnO/15°–100 ml	14.01	2.5×10^{3}	4.0×10^{-4}	1.2×10^{20}
Ga-ZnO/30°–100 ml	19.61	2.3×10^{3}	4.4×10^{-4}	0.2×10^{20}
Ga-ZnO/45°–100 ml	18.42	2.4×10^{3}	4.3×10^{-4}	1.0×10^{20}

The highest conductivity was obtained in the Ga-ZnO/15°-100 ml sample, while the lowest value was obtained in the Ga-ZnO/30°-100 ml sample. The conductivity of the Ga-ZnO/30°-100 ml sample was the least as the bulk concentration is low even when it has the highest mobility. On the other hand, the Ga-ZnO/15°-100 ml sample has the lowest mobility and highest conductivity among the samples, as it has the highest bulk concentration. As there was no significant difference in the crystallite sizes of each sample, the utmost conductivity of the Ga-ZnO/15°-100 ml sample might be due to the excellent nanostructure without structural defects such as plates that disturbs the electron propagation. We used the FTO glass substrates to get an excellent conductivity value. However, the conductivity was lower due to the two layered structure, which increases the electron scattering at layer boundaries. Evaluating the electrical conductivity measurement of a single layer in a two-layered structure is still a challenge. However, all the samples have carrier concentration and electrical conductivity of a typical transparent conductive oxide material which is in the order of 10^{20} cm^{-3} and higher than 10^{3} $\Omega^{-1}.cm^{-1}$, respectively.

4. Conclusions

In this study, we investigated the spray angle dependency for the growth of Ga-doped ZnO nanostructure by advanced spray pyrolysis deposition technique. The average top diameter and the nanostructure density of Ga-doped ZnO were 22.8 nm and 195 per μm^2, 36.9 nm and 230 per μm^2, 38.3 nm and 138 per μm^2 at spraying angles of 15°, 30°, and 45°, respectively. The physical properties of nanostructures were vastly changed with the spraying angle, as the horizontal and the vertical components of the velocity of vaporized particles were changed. Terrace-truncated nanocone structures were observed by FE-SEM images and the uniform distribution of Ga in ZnO crystal structures were confirmed by EDX mapping. According to the XRD spectra, the growth of nanostructure was favored along the c-axis, which is perpendicular to the FTO glass substrate. The highest optical transmittance of 82% in the visible range was attained by the sample prepared at the lowest spraying angle. The terrace-truncated nanocone structures support to increase the optical

transmittance by reducing the light scattering, as suggested. The optical transmittance was decreased by increasing the spraying angle, due to the formation of structural defects such as nanoplates. The foremost electrical conductivity of $2.5\times10^{3}\ \Omega^{-1}\ cm^{-1}$ was observed on the Ga-doped ZnO sample that was synthesized at the lowest spraying angle. The optimum transparent conductive oxide properties of high optical transmittance at the visible range as well as high electrical conductivity were attained by the Ga-doped ZnO nanostructure grown at the lowest spraying angle of 15^{o}.

Acknowledgments

We gratefully acknowledge Prof. Masaru Shimomura, for his great support throughout the research. We also like to show our gratitude to Dr. Hirulak Siriwardena for his support on this research paper.

References

Attanayake, S.L.B., Murakami, K., Okuya, M., 2019. Synthesis and Characterization of Al Doped ZnO Terrace-truncated Nanocone Structure by Advanced Spray Pyrolysis Deposition Technique. *Japanese Journal of Applied Physics*, Volume 58(8), pp. 080904-1–080904-3

Bandara, A., Okuya, M., Shimomura, M., Murakami, K., Rajapakse R.M.G., 2016. Effect of Spray Directions on the Crystal Growth of Fluorine-doped Tin Oxide One-dimensional Nanostructured Thin Films. *Journal of Advances in Physics*, Volume 12(1), pp. 2347–3487

Bedia, F.Z., Bedia, A., Aillerie, M., Maloufi, N., Genty, F., Benyoucef, B., 2014. Influence of Al-doped ZnO Transparent Contacts Deposited by a Spray Pyrolysis Technique on Performance of HIT Solar Cells. *Energy Procedia*, Volume 50, pp. 853–861

Bramantyo, A., Murakami, K., Okuya, M., Udhiarto, A., Poespawati, N.R., 2019. Morphological and Structural Study of Vertically Aligned Zinc Oxide Nanorods Grown on Spin Coated Seed Layers. *International Journal of Technology*, Volume 10(1), pp. 611–622

Chen, Y., Bagnall, D. M., Koh, H., Park, K., Hiraga, K., Zhu, Z., Yao, T., 1998. Plasma Assisted Molecular Beam Epitaxy of ZnO on c-plane Sapphire: Growth and Characterization. *Journal of Applied Physics*, Volume 84(7), pp. 3912–3918

Fernández, S., Gandía, J.J., 2012. Texture Optimization Process of ZnO: Al Thin Films using NH_4Cl Aqueous Solution for Applications as Antireflective Coating in Thin Film Solar Cells. *Thin Solid Films*, Volume 520(14), pp. 4698–4702

Gao, P.X., Mai, W., Wang, Z.L., 2006. Superelasticity and Nanofracture Mechanics of ZnO Nanohelices. *Nano Letters*, Volume 6(11), 2536–2543

Han, S., Akhtar, M.S., Jung, I., Yang, O., 2018. ZnO Nanoflakes Nanomaterials via Hydrothermal Process for Dye Sensitized Solar Cells. *Materials Letters*, Volume 230, pp. 92–95

Hirata, G.A., McKittrick, J., Cheeks, T., Siqueiros, J.M., Diaz, J.A., Contreras, O., 1996. Synthesis and Optelectronic Characterization of Gallium Doped Zinc Oxide Transparent Electrodes. *Thin Solid Films*, Volume 288(1–2), pp. 29–31

Hsiao, C.H., Huang, C.S., Young, S.J., Guo, J.J., Liu, C.W., Chang, S.J., 2013. Optical and Structural Properties of Ga-doped ZnO Nanorods. *Journal of Nanoscience and Nanotechnology*, Volume 13(12), pp. 8320–8324

Hu, J., Gordon, R.G., 1992. Textured Aluminum-doped Zinc Oxide Thin Films from Atmospheric Pressure Chemical-vapor Deposition. *Journal of Applied Physics*, Volume 71(2), pp. 880–890

Lao, J.Y., Huang, J.Y., Wang, D.Z., Ren, Z.F., 2003. ZnO Nanobridges and Nanonails. *Nano Letters*, Volume 3(2), pp. 235–238

Le, H.Q., Lim, S.K., Goh, G.K.L., Chua, S.J., Ong, J., 2010. Optical and Electrical Properties of Ga-Doped ZnO Single Crystalline Films Grown on $MgAl_2O_4$(111) by Low Temperature Hydrothermal Synthesis. *Journal of the Electrochemical Society*, Volume 157(8), pp. H796–H800

Li, C., Lin, Y., Li, F., Zhu, L., Sun, D., Shen, L., Chen, Y., Ruan, S., 2015. Hexagonal ZnO Nanorings: Synthesis, Formation Mechanism and Trimethylamine Sensing Properties. *RSC Advances*, Volume 5(98), pp. 80561–80567

Liu, H., Avrutin, V., Izyumskaya, N., Özgür, Ü., Morkoç, H., 2010. Transparent Conducting Oxides for Electrode Applications in Light Emitting and Absorbing Devices. *Superlattices and Microstructures*, Volume 48(5), pp. 458–484

Look, D.C., 2001. Recent Advances in ZnO Materials and Devices. *Materials Science and Engineering: B*, Volume 80(1–3), pp. 383–387

Moditswe, C., Muiva, C.M., Juma, A., 2016. Highly Conductive and Transparent Ga-doped ZnO Thin Films Deposited by Chemical Spray Pyrolysis. *Optik*, Volume 127(20), pp. 8317–8325

Rao, T.P., Kumar, M.C.S., 2010. Physical Properties of Ga-doped ZnO Thin Films by Spray Pyrolysis. *Journal of Alloys and Compounds*, Volume 506(2), pp. 788–793

Rouhi, J., Mamat, M.H., Raymond Ooi, C.H., Mahmud, S., Mahmood, M.R., 2015. High Performance Dye-sensitized Solar Cells based on Morphology-controllable Synthesis of ZnO–ZnS Heterostructure Nanocone Photoanodes. *PLoS One*, Volume 10(4), pp. 1–14

Sholehah, A., Yuwono, A.H., 2015. The Effects of Annealing Temperature and Seed Layer on the Growth of ZnO Nanorods in a Chemical Bath Deposition Process. *International Journal of Technology*, Volume 6(4), pp. 565–572

Visser, D., Ye, Z., Prajapati, C.S., Bhat, N., Anand, S., 2017. Investigations of Sol-Gel ZnO Films Nanostructured by Reactive Ion Beam Etching for Broadband Anti-reflection. *ECS Journal of Solid State Science and Technology*, Volume 6(9), pp. P653–P659

Wu, G.M., Lin, H.H., Lu, H.C., 2008. Work Function and Valence Band Structure of Tin-doped Indium Oxide Thin Films for OLEDs. *Vacuum*, Volume 82(12), pp. 1371–1374

Yadav, A.A., Barote, M.A., Masumdar, E.U., 2010. Studies on Nanocrystalline Cadmium Sulphide (CdS) Thin Films Deposited by Spray Pyrolysis. *Solid State Sciences*, Volume 12(5), pp. 1173–1177

Yan, M., Zhang, Q., Zhao, Y., Yang, J., Yang, T., Zhang, J., Li, X., 2015. Applications of Transparent Conducting Oxides in Organic Light Emitting Devices. *Journal of Nanoscience and Nanotechnology*, Volume 15(9), pp. 6279–6294

Yim, K., Kim, H.W., Lee, C., 2007. Effects of Annealing on Structure, Resistivity and Transmittance of Ga-doped ZnO Films. *Materials Science and Technology*, Volume 23(1), pp. 108–112

Yin, Z., Liu, X., Wu, Y., Hao, X., Xu, X., 2012. Enhancement of Light Extraction in GaN-based Light-emitting Diodes using Rough Beveled ZnO Nanocone Arrays. *Optics Express*, Volume 20(2), pp. 1013–1021